UDE-Based Current Controller With Enhanced Grid Frequency Fluctuation Adaptability for *LCL*-Type Grid-Tied Inverters

Yongkang Xiong, Yongqiang Ye, *Senior Member, IEEE*, and Mingzhe Zhu

***Abstract*—The uncertainty and disturbance estimator (UDE) with a time delay filter has been widely used for inverter systems due to its satisfactory harmonic rejection performance. However, the control performance may be affected when the grid frequency fluctuates. In this article, a modified UDE (FUDE) is proposed to improve the grid frequency fluctuation adaptability of the LCL grid-tied inverter systems, which contains a compound filter consisting of time delay, zero-phase low-pass, and high-pass filters. Compared with the traditional time delay UDE, it can offer a wider notch bandwidth at the selected frequencies. A dual-loop controller is built in the separate-structure-type UDE-based controller, containing an outer loop PR controller and an inner loop FUDE. The sufficient conditions for the system stability are obtained by the small-gain theorem. The comparison experiments of the dual-loop controller with the proposed FUDE and the conventional time delay zero-phase low-pass UDE are performed on a 2-kW experimental platform, and the results demonstrate the effectiveness of the proposed FUDE.**

***Index Terms*—Grid frequency fluctuation adaptability, high-pass filter, *LCL*-type grid-tied inverters, time delay filter, uncertainty and disturbance estimator (UDE).**

I. Introduction

THE LCL-type grid-tied inverter is usually selected as the interface between a direct current (dc) and an alternating current (ac) power grid. However, a resonance exists in the LCL filter, which may cause the system to be unstable [1]. To suppress the resonance of the LCL filter, a common method is to introduce damping in the inverter system. Many damping approaches have been proposed in the literature, which can be mainly divided into passive damping and active damping (AD) methods. AD methods have become popular, benefiting from their low cost. The capacitor current feedback AD is widely used among those AD techniques due to its simple structure [2]. After the damping is appropriately designed, the LCL can be approximated as the L within the control bandwidth [3]. In addition to the instability problem caused by the resonance of the LCL filter, there are many uncertainties and disturbances in the inverter [4], which will affect the control performance of the injected current and power quality.

There are feedback and disturbance rejection controls in the literature for controlling the injected current. The feedback control mainly includes the proportional integral control [5], proportional resonant (PR) control [6], repetitive control [7], and so on [8]. The disturbance rejection control mainly includes the disturbance observer-based control [4], active disturbance rejection control [9], uncertainty and disturbance estimator (UDE)-based control [10], and so on. The main difference between the feedback and the disturbance rejection controls lies in the idea of processing methods for the system disturbance and uncertainty. In feedback control, the nonideal factors of the system are regarded as the reference tracking error, which is eliminated through the feedback control law, i.e., the influence of the system nonideal factors on the output can be eliminated by the feedback control. However, the nonideal factors of the system are actively considered in the disturbance rejection control through the known part or measurable part of the system, and the corresponding compensation is introduced in control to eliminate the influence of the system's nonideal factors on the output. To explore the mechanism of inverter disturbance suppression, much research has been done in the literature with uncertainty and disturbance rejection techniques [11]. Compared to the conventional feedback control, the disturbance rejection control provides more guidance on intuitive design for eliminating the known and unknown disturbances in the inverters, which are lumped together in the disturbance rejection control, and the expression of the lumped disturbance rejection function can also be obtained intuitively. This intuitive expression is unavailable in traditional feedback control considering the difficulty of modeling the system uncertainty directly in feedback control.

UDE, one of uncertainty and disturbance rejection techniques, has been widely investigated and applied in varieties of applications [12], [13], [14], [15]. The basic idea of the UDE is to use the known and measurable variables to estimate the lumped uncertainty and disturbance of the system, and then establish a corresponding compensation in control to eliminate the influence of disturbances and uncertainties on the system [16]. There

Manuscript received 3 January 2022; revised 31 March 2022, 9 July 2022, and 5 September 2022; accepted 10 October 2022. Date of publication 14 October 2022; date of current version 18 November 2022. This work was supported in part by the National Natural Science Foundation of China under Grant 52267016 and Grant 61973157. Recommended for publication by Associate Editor J. Liu. *(Corresponding author: Yongkang Xiong.)*

Yongkang Xiong is with the Information Engineering School, Nanchang University, Nanchang 330031, China (e-mail: yongkang_xiong@foxmail.com).

Yongqiang Ye is with the College of Automation Engineering, Nanjing University of Aeronautics and Astronautics, Nanjing 211106, China (e-mail: yongqiang_leaf@hotmail.com).

Mingzhe Zhu is with the School of Electric power Engineering, Nanjing Institute of Technology, Nanjing 210094, China (e-mail: zhumingzhe1991@126.com).

Color versions of one or more figures in this article are available at https://doi.org/10.1109/TPEL.2022.3214682.

Digital Object Identifier 10.1109/TPEL.2022.3214682

are two types of UDE in the literature: 1) the separate-structure-type UDE (SUDE); and 2) the reference-model-tracking-type UDE (RUDE). Although both UDEs have two degrees-of-freedom structures and their basic ideas are similar, their implementations are quite different. In the RUDE, a desired closed-loop transfer function needs to be designed primarily, and there is only one control loop in the system. Although it is not necessary to design the desired closed-loop transfer function in the SUDE, there are two loops that need to be designed separately [17].

By reasonably designing the controller parameters, both UDEs can eliminate the influence of uncertainty and disturbance on the system. In [14], a RUDE form control strategy with a simple tuning algorithm was proposed for an $LCCL$-type grid-tied inverter against system parameter uncertainties. However, the quality of the injected current was unsatisfactory due to the limited notch depth. To improve the quality of the injected current, a time delay filter was used in the UDE; with the help of the time delay unit, the notch depth of the UDE is deeper at specific frequencies [10], [18]. In [19], a compound filter was used in the UDE-based controller to improve the disturbance rejection performance of the inverter system. However, the specific frequencies do not match harmonic frequencies as an infinite impulse response (IIR) was used in [10], [18], [19], which affects the performance of the disturbance rejection. To improve the rejection of the disturbances further, a finite impulse response (FIR) time delay filter was adopted in the RUDE and SUDE [3], [17]. The difference was discussed in [17], and both of them can achieve satisfactory performance under the fixed grid frequency condition. In practice, however, the grid frequency is usually variable in a certain range [20], especially in the case of the low-voltage microgrid where the grid frequency fluctuation exceeds 1.0 Hz [26], which was not discussed in [3] and [17]. The grid frequency fluctuations will affect the systems performance because the notch bandwidth of the time delay UDE control at the selected frequency is fixed due to the selected filter. Thus, it is meaningful to study the UDE design method of LCL-type grid-tied inverters in the consideration of the grid frequency fluctuation.

In this article, an IIR high-pass filter is introduced to the traditional FIR time delay UDE for the grid-tied inverters, and a notch coefficient is designed to compensate for the system's stability. Then, a dual-loop control structure is built for LCL-type grid-tied inverters; the proposed enhanced grid frequency fluctuation adaptable UDE (FUDE) is used as the inner loop controller, which employs a time delay, high-pass, and low-pass compound filter; the same as [17], a PR controller is used as the outer loop controller. Also, according to the small-gain theorem, the stability criterion for the proposed compound controller is proposed in detail. The main contributions of this article are as follows.

1) Compared with the traditional time delay UDE, the bandwidth of the notch frequencies of the proposed FUDE become wider with which the curve of the total harmonic distortion (THD) in the injected current is flat in a large grid frequency fluctuation range.
2) The notch depth of the system in low-frequency range is also deeper with the use of the high-pass filter.

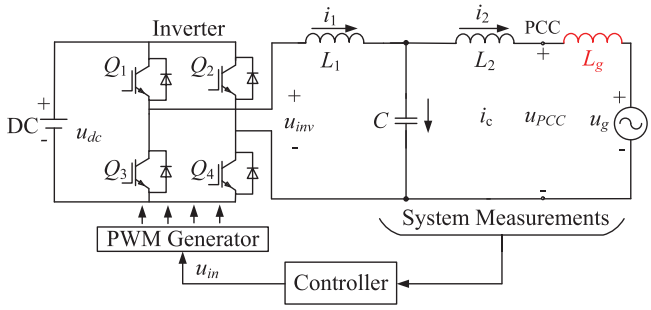

Fig. 1. System topology of a grid-tied inverter with an LCL filter.

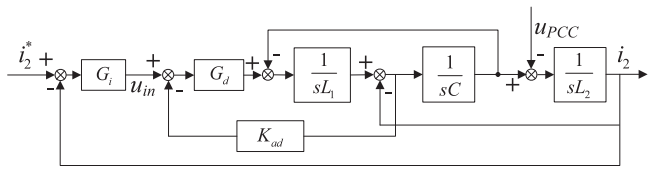

Fig. 2. Diagram of the LCL grid-tied inverter with capacitor-current-feedback AD.

TABLE I
EXPERIMENT PARAMETERS

Parameter	Value	Parameter	Value
DC bus voltage u_{dc}	380 V	PCC voltage u_{PCC}	220 V
PWM frequency f_c	10 kHz	Sampling period T_s	50 μs
Inverter-side inductor L_1	3 mH	Grid-side inductor L_2	2 mH
Capacitor C	6 μF		

3) The freedom to adjust the system's stability is increased by introducing the notch coefficient.

II. MODELING OF THE LCL-TYPE GRID-TIED INVERTER WITH THE AD

A. Modeling of the LCL-Type Grid-Tied Inverter

Fig. 1 shows the topology of a single-phase grid-tied inverter with an LCL filter, where u_{dc}, u_{inv}, u_{in}, u_{PCC}, u_g, L_1, L_2, and C are the dc bus voltage, the input voltage of the LCL filter, the controller output, the voltage of the point of common coupling (PCC), the grid, the inverter-side inductor, the grid-side inductor, and the filter capacitor, respectively. The diagram of the LCL grid-tied inverter with the capacitor-current-feedback AD can be obtained as shown in Fig. 2, where K_{ad} is the AD coefficient, $G_i(s)$ is a feedback controller, and $G_d(s)$ is the pulsewidth modulation (PWM) gain k_{pwm} (which is unity gain in this article) multiplied by one sampling period computation plus the half sampling period PWM delays [i.e., $G_d(s) = k_{\mathrm{pwm}} e^{-1.5T_s s}$, with T_s is the sampling period] [21].

According to Fig. 2, the transfer function from the controller output u_{in} to the injected current i_2 can be derived as

$$\frac{i_2(s)}{u_{\mathrm{in}}(s)} = \frac{e^{-1.5T_s s}}{s^3 L_1 L_2 C + s^2 L_2 C K_{\mathrm{ad}} e^{-1.5T_s s} + s(L_1 + L_2)}. \tag{1}$$

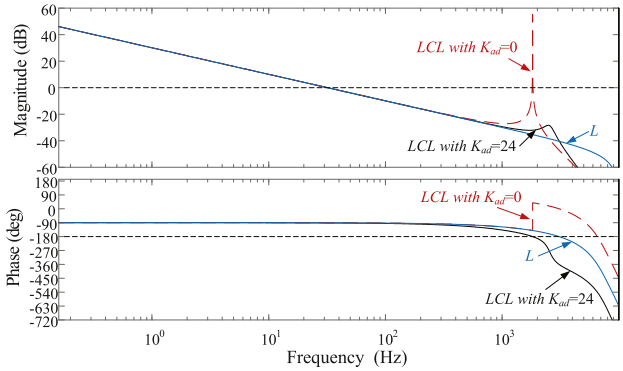

Fig. 3. Bode diagram of the LCL grid-tied inverter with and without AD.

B. AD for the LCL Filter

The parameters of the inverter are listed in Table I, and $e^{-1.5T_s s}$ is approximated by a third-order Pade approximation [14]. Fig. 3 shows the frequency responses of the L filter and LCL filter with and without AD, and the AD coefficient K_{ad} is selected as 24 here (the detailed design of the AD coefficient can be obtained by referring to [22]). The figure suggests that AD could effectively attenuate the resonant peak, and make the LCL filter behave much similar to the L filter in the low- and mid-frequency regions.

III. FUDE-Based Current Control Strategy

For the grid-tied inverter (as shown in Fig. 2), (1) needs to be considered in the whole design process if a conventional feedback controller is built. However, according to [16], a nominal plant instead of (1) is used in the UDE-based controller design. The difference between the nominal plant and the actual plant is considered as the uncertainty of the nominal plant, and the aim of the UDE is to make the actual plant present as a nominal plant without nonideal factors.

A. Time-Delay-Based UDE Current Control Scheme

1) Basic Idea of the UDE-Based Current Control: Referring to [3] and according to Fig. 3, the L filter can be chosen as the nominal plant [i.e., (2)] since the L filter has almost the same property as the LCL filter in the low- and mid-frequency regions.

$$\frac{i_2(s)}{u_{\text{in}}(s)} = \frac{1}{s(L_1+L_2)}. \tag{2}$$

Following the step proposed in [3] and [17], the voltage equation of the L filter inverter with unity PWM gain can be derived as

$$L\frac{\mathrm{d}i_2(t)}{\mathrm{d}t} = u_{\text{in}}(t) - u_{\text{PCC}}(t) \tag{3}$$

where $L = L_1 + L_2$. In line with the UDE scheme [16], [17], the state equation of the inverter with disturbance and uncertainty can be expressed as

$$\dot{i}_2(t) = \Delta a i_2(t) + (L^{-1} + \Delta b)u_{\text{in}}(t) + d(t) \tag{4}$$

where Δa and Δb are the unknown dynamic coefficients of the grid-tied inverter and $d(t)$ consists of the known [e.g., $-L^{-1}u_{\text{PCC}}(t)$] and unknown disturbances. According to the idea of the SUDE, the nonideal factors in (4) can be unified as the total uncertainty and disturbance (TUD), and then rejected by a part of u_{in} [17]. Following the method above, the state function (4) can be rewritten as follows:

$$\dot{i}_2(t) = L^{-1}[u_t(t) - u_d(t) + f(t)] \tag{5}$$

where

$$\begin{cases} u_t(t) - u_d(t) = u_{\text{in}}(t) \\ f(t) = L[\Delta a i_2(t) + \Delta b u_{\text{in}}(t) + d(t)] \end{cases} \tag{6}$$

where $u_t(t)$, $u_d(t)$, and $f(t)$ represent the output of the tracking controller, the output of the disturbance and uncertainty estimator, and the TUD, respectively. When $u_d(t) \approx f(t)$ establishes, (5) will be equal to (2) (in the same domain), and the rest of (5) will be

$$\dot{i}_2(t) = L^{-1}u_t(t) \tag{7}$$

which is the nominal plant, i.e., the actual plant is regulated as the nominal plant in this case. Thus, the $u_d(t)$ design is essential to the SUDE. Referring to (4), $f(t)$ can be got as

$$f(t) = L\dot{i}_2(t) - u_t(t) + u_d(t). \tag{8}$$

According to [17], (8) cannot be used directly to represent $u_d(t)$ because $\dot{i}_2(t)$ is not causal and will amplify the measurement noise [17]. Thus, $u_d(t)$ can be obtained by introducing a filter to $f(t)$ [16], i.e.,

$$u_d(t) = f_e(t) = f(t) * g_f(t) \tag{9}$$

where $g_f(t)$ is a filter, $f_e(t)$ is the estimate of $f(t)$, and $*$ is the convolution operator. With this operation, $u_d(t)$ becomes realizable. By combining (8) and (9) as well as taking the Laplace transform, $u_d(t)$ in the s domain can be expressed as

$$u_d(s) = [Lsi_2(s) - u_t(s)]\frac{g_f(s)}{1-g_f(s)}. \tag{10}$$

According to (10), the basic structure of the SUDE-based controller can be obtained as shown in Fig. 4 where the actual plant consists of the nominal plant $1/Ls$ and the unmodeled dynamics $\Delta P(s)$. An inner loop controller (i.e., SUDE) and an outer loop controller (i.e., G_i) are included in the SUDE-based controller. It is easy to design the outer loop controller because the actual plant acts as the nominal one when the inner loop SUDE controller is appropriately designed.

Recalling the abovementioned design and Fig. 4, the SUDE can be easily implemented when g_f is selected. Combining (5)

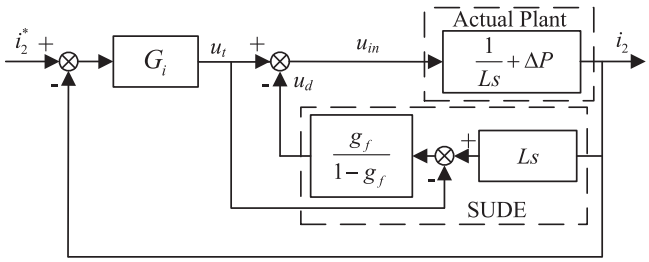

Fig. 4. Diagram of the LCL grid-tied inverter with UDE.

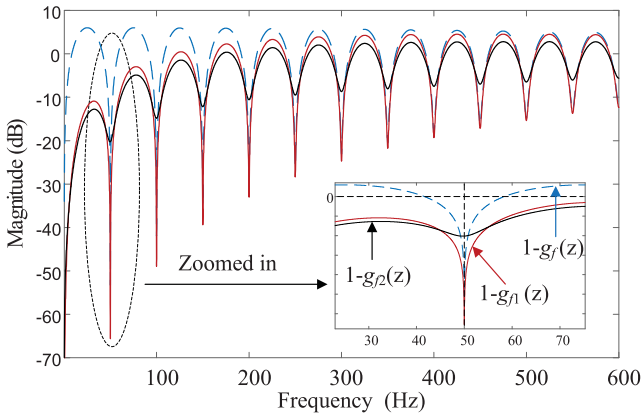

Fig. 5. Bode diagrams of $1-g_f(z)$, $1-g_{f1}(z)$, and $1-g_{f2}(z)$.

and (8) as well as taking the Laplace transform, we can have

$$si_2(s) = L^{-1}\{u_t(s) + [1-g_f(s)]f(s)\}. \tag{11}$$

As indicated in (11), the influence of $f(s)$ on $i_2(s)$ is directly constrained by $1-g_f(s)$. The selection of $1-g_f(s)$ has a significant influence on the control performance of $i_2(s)$.

2) Time Delay Filter-Based UDE: For inverters, in the literature, the UDE with a time delay low-pass filter can provide better control performance than a conventional low-pass filter because the time delay form UDE can offer a stronger attenuation at specific harmonics. As stated in [10] and [17], the time delay form UDE is implemented in two ways: a) IIR time delay low-pass filter way; or b) FIR time delay zero-phase low-pass filter way, and the FIR time delay low-pass filter can provide better harmonic rejection capability (the differences between these two implementations have been discussed in [17]). The z domain expression of the FIR time delay low-pass filter in [17] is

$$g_f(z) = z^{-400} g_{\text{low}}(z) \tag{12}$$

where 400 is the result of the sampling frequency divided by the grid frequency and $g_{\text{low}}(z)$ is a zero-phase low-pass filter, which can be expressed as

$$g_{\text{low}}(z) = i(0) + \sum_{1}^{n} i(k)(z^k + z^{-k}) \tag{13}$$

where n is half of the order of $g_{\text{low}}(z)$ and $i(k)$ is the filter's coefficient, which is given in the Appendix. The dashed line in Fig. 5 shows the bode diagram of $1-g_f(z)$; as indicated in this figure, $1-g_f(z)$ acts as a notch filter at the harmonic frequencies, which means that $f(z)$ [the z domain counterpart of $f(s)$] will be significantly suppressed by the FIR time delay low-pass filter. However, it can be found that the notch bandwidth of the $1-g_f(z)$ is narrow, i.e., the rejection of the harmonics will be affected by the grid frequency fluctuations [17].

B. Proposed Enhanced Grid Frequency FUDE-Based Current Control Scheme

1) FUDE: According to [19], an IIR high-pass filter can be used to reduce the low-frequency gain of $1-g_f(z)$ with which the control performance is improved. However, the low-pass filter in [19] is designed in IIR form, which causes the notch frequencies to be inconsistent with the harmonic frequency within the high-frequency range of the bandwidth. Here, to avoid the shortcoming brought by the IIR time delay low-pass filter, an FIR time delay low-pass filter with a high-pass filter is proposed and expressed as

$$h(z) = g_{\text{hi}}(z)[1-g_f(z)] \tag{14}$$

where $h(z)$ and $g_{\text{hi}}(z)$ are the TUD rejection and high-pass filters, respectively. The corresponding filter $g_{f1}(z)$ of $h(z)$ can be obtained as

$$g_{f1}(z) = 1-h(z) = 1-g_{\text{hi}}(z) + g_{\text{hi}}(z)g_f(z). \tag{15}$$

The solid line in Fig. 5 shows the bode diagram of $1-g_{f1}(z)$; as indicated in the figure, the gain of $1-g_{f1}(z)$ is smaller compared with that of $1-g_f(z)$ within the low-frequency range, which means that with $g_{\text{hi}}(z)$ introduced, the low-frequency harmonics can be rejected greater [19]. Different from [19], the notch matches the harmonic frequencies when $g_{f1}(z)$ with the FIR filter is used. In addition, it can be found that the notch bandwidth of $1-g_{f1}(z)$ is improved within the low-frequency range. However, the system stability will be affected with the high-pass filter used. Thus, a coefficient is introduced in the SUDE to improve the system stability, then noting (12), the $g_{f1}(z)$ can be modified as

$$g_{f2}(z) = 1-g_{\text{hi}}(z) - Qg_{\text{hi}}(z)g_{\text{low}}(z)z^{-400} \tag{16}$$

where Q is the notch coefficient. Fig. 5 shows the bode diagrams of $1-g_f(z)$, $1-g_{f1}(z)$, and $1-g_{f2}(z)$, respectively, and the UDE with $g_{f1}(z)$ or $g_{f2}(z)$ is named FUDE in this article. As indicated in Fig. 5, although the notch depth of $1-g_f(z)$ is deeper than that of $1-g_{f2}(z)$, the notch bandwidth of $1-g_{f2}(z)$ at selected frequencies is wider than that of $1-g_f(z)$. Moreover, it can be found that the notch depth of $1-g_{f1}(z)$ is the deepest among the three cases, and the notch width is also relatively wide. It can be inferred from the notch performance that $g_{f1}(z)$ seems to be the best choice among the three filters. However, the stability of the FUDE with $g_{f1}(z)$ is the worst among them, and Q can be considered as a compromise to improve the stability. The detailed stability analysis will be discussed in Section III-D.

2) PR Controller: With the reasonable designed FUDE adopted, $f(z)$ can be significantly rejected by $1-g_{f2}(z)$, and the actual system is approximated as a nominal system. A PR controller is employed for the nominal system in this article, which is shown as follows:

$$G_i(s) = K_p + \frac{2K_r\omega_i s}{s^2 + 2\omega_i s + \omega_o^2} \tag{17}$$

where $\omega_o = 2\pi f_o$ is the fundamental angular frequency, ω_i is the resonant cutoff frequency, which is the bandwidth of the resonant part, and a typical value of ω_i is π rad/s (i.e., there is a 1% variation of $2\pi f_o$) [23]. According to [17], the proportional gain K_p and the resonant gain K_r can be selected as 15 and 800, respectively.

C. Stability Study

According to Fig. 4 and replacing $g_f(z)$ with $g_{f2}(z)$, the closed-loop transfer function of the system can be derived and expressed as

$$G_{\mathrm{cl}}(z)=\frac{i_2(z)}{i_2^*(z)}=\frac{G_i(z)P(z)}{1-g_{f2}(z)+\dfrac{g_{f2}(z)P(z)}{P_0(z)}+G_i(z)P(z)} \tag{18}$$

where $P(z)$ and $P_0(z)$ are the actual and the nominal plants, respectively. The terms in (18) are as follows, (19) shown at the bottom of the page.

It is difficult to accurately get the poles of the closed-loop transfer function $G_{\mathrm{cl}}(z)$ because the order of the denominator of (18) is very high. Thus, we can divide (18) into two parts as

$$G_{\mathrm{cl}}(z)=\frac{G_i(z)P(z)}{1+G_i(z)P(z)}\frac{1}{1+\dfrac{\dfrac{g_{f2}(z)P(z)}{P_0(z)}-g_{f2}(z)}{1+G_i(z)P(z)}}. \tag{20}$$

According to the small-gain theorem [24], sufficient conditions for system stability can be obtained as follows.

1) $\dfrac{G_i(z)P(z)}{1+G_i(z)P(z)}$ is stable.
2) $\left\|\dfrac{\dfrac{g_{f2}(z)P(z)}{P_0(s)}-g_{f2}(z)}{1+G_i(z)P(z)}\right\|_\infty<1 \quad \forall z=e^{j\omega}, 0<\omega<\dfrac{\pi}{T_s}$.

Equation (20) suggests that the stability of the inverter system is up to two conditions, i.e., conditions 1) and 2).

Remark 1: Condition 1) is the closed-loop transfer function of the actual plant $P(z)$ with the outer loop controller [i.e., PR controller $G_i(z)$], whose stability can be obtained by the poles map of the closed-loop transfer function.

Remark 2: Condition 2) is relevant to all terms of the inverter system, and it is worth noting that condition 2) will always establish when $P(z)=P_0(z)$.

To summarize, the stability of the inverter system is up to $P(z)$ only when $G_i(z)$, $P_0(z)$, and $g_{f2}(z)$ are designed and selected well.

D. Grid Impedance Robustness and Parameter Design

In practice, as shown in Fig. 1, the power grid is not an ideal voltage source, but a voltage source and impedance (L_g) series structure (the weak grid condition) [17], [25], which means that $P(z)$ will change with L_g under the weak grid condition, and

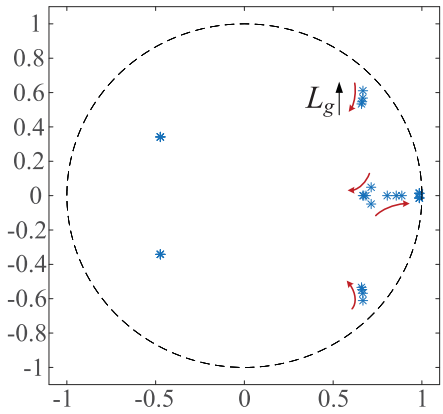

Fig. 6. Poles of condition 1) with L_g changes from 0 to 3 mH.

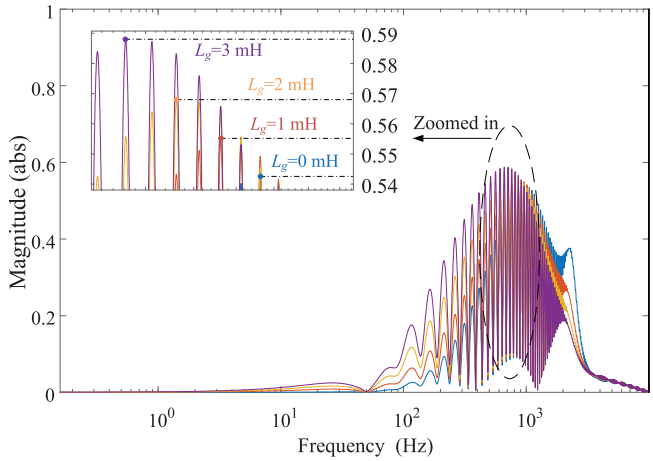

Fig. 7. Stability condition 2) with L_g changes from 0 to 3 mH.

L_g can be regarded as the uncertainty of $P(z)$. Thus, the change of stability conditions with L_g is selected to study the stability of the inverter system. According to [17], L_g can be emulated by increasing L_2. Then, the results of conditions 1) and 2) with L_g changes can be obtained in Figs. 6 and 7.

As indicated in Figs. 6 and 7, both conditions 1) and 2) keep established when L_g changes from 0 to 3 mH, i.e., the proposed inverter system can adapt to the change of L_g from 0 to 3 mH.

As shown in Fig. 5, the notch depth of $1-g_{f1}$ is deeper than that of $1-g_{f2}$, i.e., the TUD with $1-g_{f1}$ will be attenuated greater than $1-g_{f2}$ at the selected frequencies. However, according to stability condition 2), the system's stability varies with g_f. Fig. 8 shows the stability condition 2) with different g_f, there are three lines in the figure representing the influence

$$\begin{cases} P(z)=\mathcal{Z}\left[\dfrac{1}{s^3L_1L_2C+s^2L_2CK_{\mathrm{ad}}e^{-1.5T_ss}+s(L_1+L_2)}\right]z^{-1.5} \\ P_0(z)=\mathcal{Z}\left[\dfrac{1}{s(L_1+L_2)}\right] \\ G_i(z)=K_p+\mathcal{Z}\left[\dfrac{2K_r\pi s}{s^2+2\pi s+(100\pi)^2}\right] \\ g_{f2}(z)=1-g_{\mathrm{hi}}(z)-Qg_{\mathrm{hi}}(z)g_{\mathrm{low}}(z)z^{-400} \end{cases}. \tag{19}$$

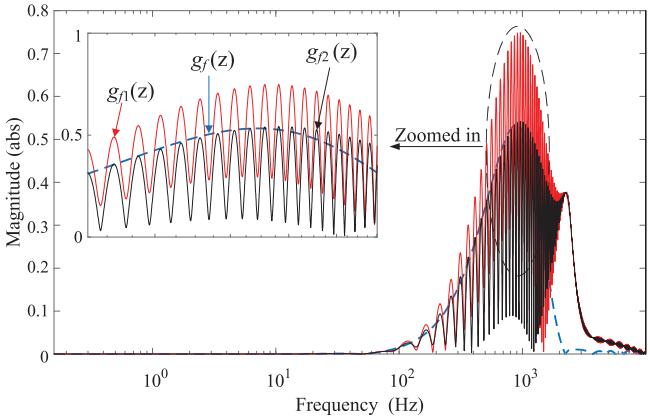

Fig. 8. Stability condition 2) with different g_f.

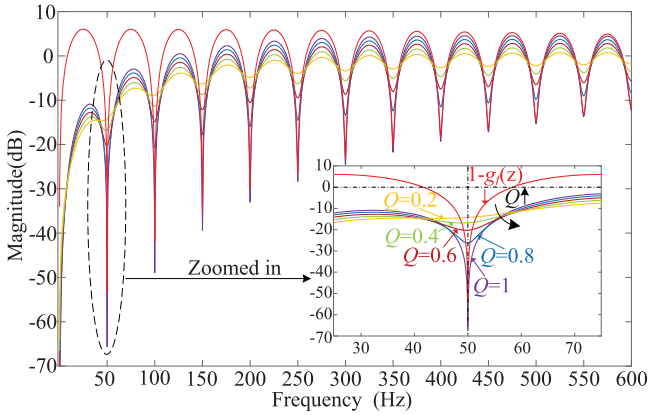

Fig. 9. Bode diagrams of $1-g_f(z)$, $1-g_{f1}(z)$, and $1-g_{f2}(z)$ with different Q.

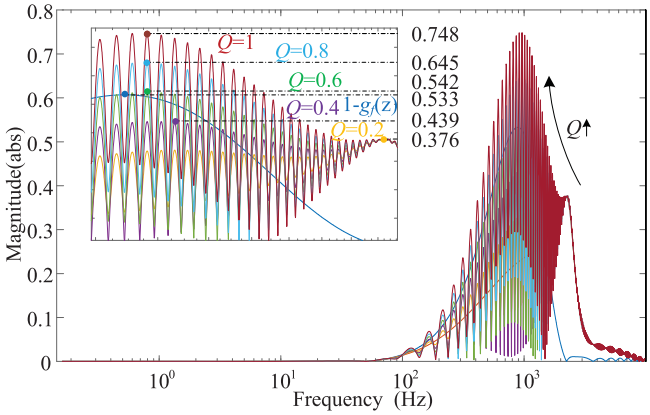

Fig. 10. Bode diagrams of stability condition 2) with $g_f(z)$, $1-g_{f1}(z)$, and $g_{f_2}(z)$ under different Q.

of three different filters on the stability condition 2). It can be found that the peak value of the lines with $1-g_f$ and $1-g_{f2}$ is close, while the peak value with $1-g_{f1}$ is significantly higher. Thus, the notch coefficient Q less than 1 is designed to make the system stable enough. The relationship between the selection of Q and stability condition 2) is studied as follows.

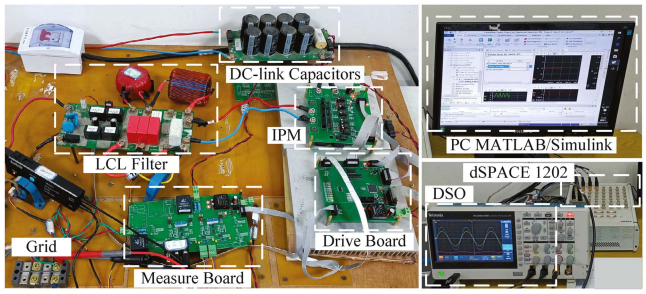

Fig. 11. Experimental setup.

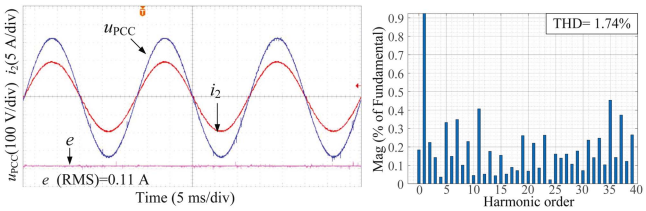

Fig. 12. Result of the SUDE control. (a) Injected current i_2. (b) Spectrum of the injected current.

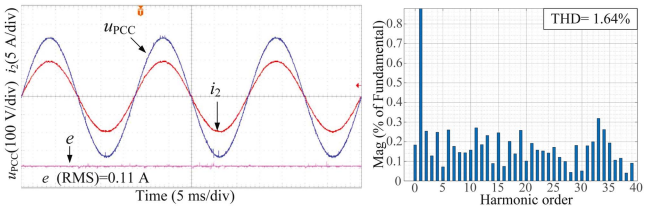

Fig. 13. Result of the FUDE control with $Q=1$. (a) Injected current i_2. (b) Spectrum of the injected current.

Figs. 9 and 10 show the disturbance rejection function and stability condition 2) with different filters, especially for different Q. As indicated in Fig. 9, the larger of Q, the better the rejection performance. However, as shown in Fig. 10, the peak value of stable condition 2) increases with Q, which means that stability of the system cannot be guaranteed when Q is designed unsuitable. Thus, the selection of Q should tradeoff the rejection performance and the system stability. For the proposed inverter systems, we select $Q=0.6$, as the peak values of stable condition 2) of $1-g_f(z)$ and $1-g_{f2}(z)$ with $Q=0.6$ are similar, as shown in Fig. 10, which means that the stability of UDE with $g_f(z)$ does not become worse with FUDE used, while the notch bandwidth is wider, as shown in Fig. 9.

IV. Experimental Verification

The effectiveness of the proposed FUDE is verified on the 2-kW LCL grid-tied inverter prototype, which consists of an insulated gate bipolar transistor inverter bridge, an LCL filter, a voltage sensor used in the phase-locked loop, and two current sensors for i_c and i_2. The single-phase grid-tied inverter is controlled by a dSPACE DS-1202 controller, which is connected with a PC running MATLAB/Simulink and ControlDesk. A

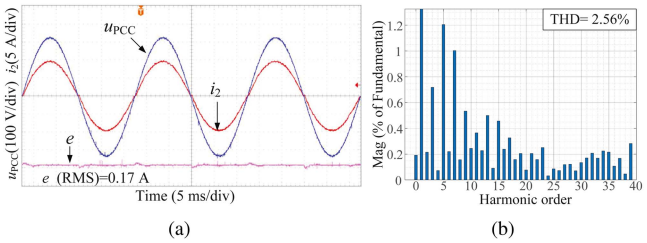

Fig. 14. Result of the FUDE control with $Q = 0.6$. (a) Injected current i_2. (b) Spectrum of the injected current.

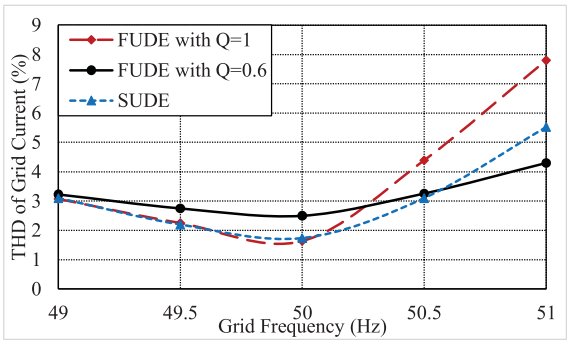

Fig. 15. THDs of the injected current with the variation of grid frequency.

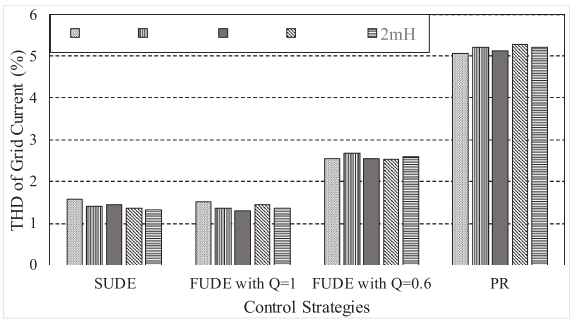

Fig. 16. THDs of the injected current under different control strategies with the variation of added L_g.

Chroma 62100H-1000 programmable ac voltage source is configured to simulate the grid. The experimental setup is shown in Fig. 11.

A. Experimental Results

In this section, the experiments including steady-state response, dynamic response, and robustness experiments will be done, and all controller parameters are given in previous sections.

1) Steady-State Response Experiments: Figs. 12–14 show the waveforms and spectra of three controls with 10-A reference current, respectively. As indicated in the figures, the steady-state control performance of the SUDE-based [with $g_f(z)$] and proposed FUDE-based with $Q = 1$ controls on the injected current is similar in general because the notch depths of $1 - g_f(z)$ and $1 - g_{f1}(z)$ are similar at the harmonic frequencies. Relatively, the control performance of the FUDE with $Q = 1$ is slightly better since the notch depth is deeper within the low-frequency region (see Fig. 5). Meanwhile, the performance of the SUDE

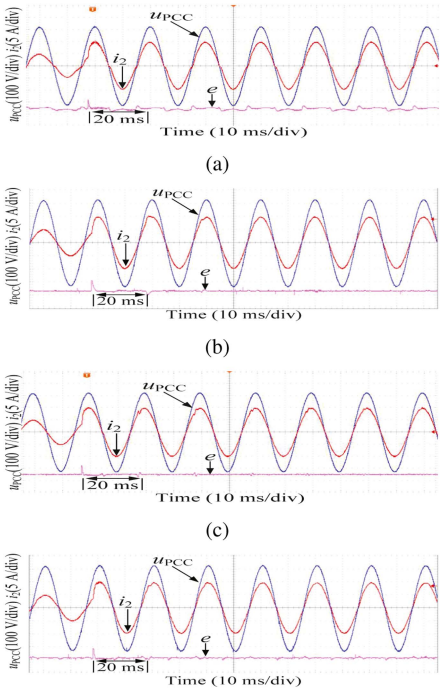

Fig. 17. Dynamic responses of different controls when $f_g = 50$ Hz. (a) PR control. (b) PR with SUDE control. (c) PR with FUDE control with $Q = 1$. (d) PR with FUDE control with $Q = 0.6$.

control with $Q = 0.6$ is worse than the other two controls, which can be attributed to the shallower notch depth of $1 - g_{f2}(z)$ (see Fig. 5).

2) Robustness Experiments: Recalling the design of the proposed controller, the grid frequency fluctuation adaptability of the proposed FUDE- and the SUDE-based controls are the main difference between the two UDE-based controls. In this section, we will investigate two kinds of robustness performance of the two UDE-based controls: a) the robustness performance to the variation of the grid frequency; and b) the robustness performance to the grid impedance variation.

To study the grid frequency fluctuation adaptability of the two UDE-based controls, we change the fundamental frequency of the ac source from 49 to 51 Hz, and the results can be found in Fig. 15. As shown in the figure, there is a significant difference between the two UDE-based controls for the robustness performance to the grid frequency fluctuation. The THD fluctuations of the injected current with the SUDE-based controller become more remarkable than that with the FUDE-based controller when the grid frequency f_g deviates from the 50 Hz, and the larger of the deviation, the greater of the THD fluctuations, i.e., compared to the SUDE-based control, the proposed FUDE-based control can adapt a broader range of grid frequency fluctuations. Relatively, the inverter system has better grid frequency fluctuation adaptability when Q in the proposed FUDE set to 0.6, which can be inferred from the results shown in Fig. 5. In addition, the THD curve of the FUDE strategy with $Q = 0.6$ is flat in a large power grid frequency range, although the THD is not the lowest in the frequency within 50.5 Hz. The proposed strategy

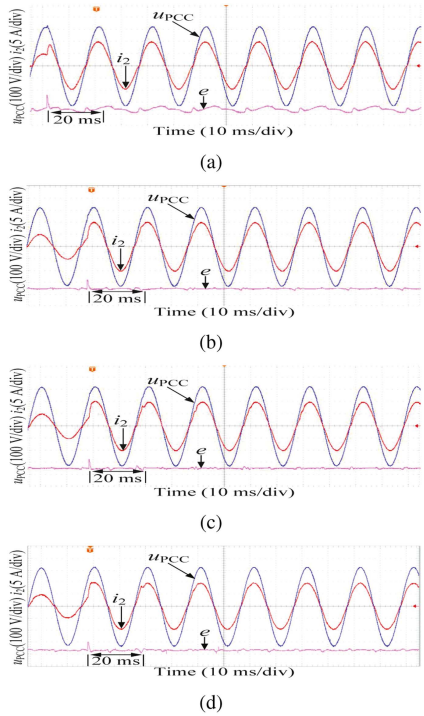

Fig. 18. Dynamic responses of different controls when $f_g = 49$ Hz and $L_g = 1$ mH. (a) PR control. (b) PR with SUDE control. (c) PR with FUDE control with $Q = 1$. (d) PR with FUDE control with $Q = 0.6$.

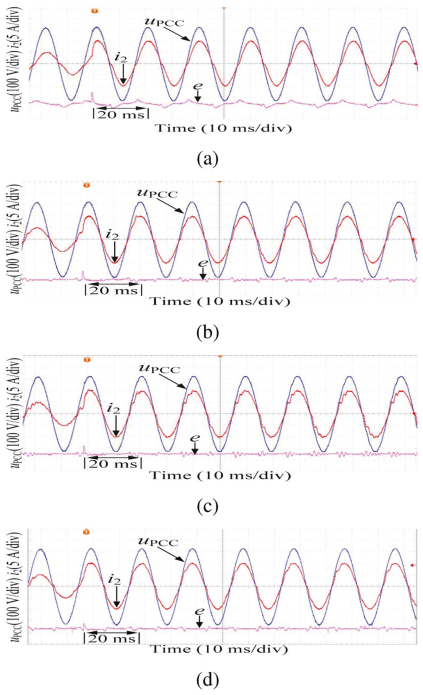

Fig. 19. Dynamic responses of different controls when $f_g = 51$ Hz and $L_g = 1$ mH. (a) PR control. (b) PR with SUDE control. (c) PR with FUDE control with $Q = 1$. (d) PR with FUDE control with $Q = 0.6$.

makes a tradeoff between the notch depth and the notch width at the selected frequency, i.e., a tradeoff between the disturbance rejection and the stability performance is made by introducing the notch coefficient. As a result, the system design degree of freedom is higher and the notch bandwidth at the selected frequency becomes adjustable. Furthermore, using the proposed FUDE control can alleviate the deterioration of inverter power output quality under a wide range of grid frequency fluctuations, specifically for the grid frequency fluctuation exceeding 1.0 Hz.

To verify the robustness performance of the FUDE with $Q = 0.6$ to the grid impedance variation, an external inductor L_g is added between the PCC and the ac source.

As shown in Fig. 16, the performance of the proposed control strategy is similar to that of the comparison control strategies, that is, it can adapt to the change of grid impedance under 2 mH, although there are some differences in their THDs.

3) Dynamic Response Experiments: To verify the dynamic responses performance of the proposed and compared controls, we also provide the dynamic response comparison results in three cases: a) $f_g = 50$ Hz; b) $f_g = 49$ Hz, $L_g = 1$ mH; and c) $f_g = 51$ Hz, $L_g = 1$ mH. The comparison controls are PR control, PR + SUDE control, PR + FUDE ($Q = 1$) control, and PR + FUDE ($Q = 0.6$) control, respectively. As the experimental results show in Figs. 17–19, the response times of the four controls are similar when the reference current steps from 5 to 10 A, but the PR control performance is the worst. The stability of PR + FUDE ($Q = 1$) is the worst with which the waveform even has a certain oscillation when $f_g = 51$ Hz and $L_g = 1$ mH. Moreover, it can be concluded from the robustness and dynamic responses experiments that the dynamic and steady-state performance of the proposed FUDE (with $Q = 0.6$) can be guaranteed in the case of the grid frequency fluctuation with the grid impedance variation to a certain range.

V. Conclusion

In this article, an enhanced grid frequency FUDE-based controller compounded by an outer loop PR controller and an inner loop FUDE was proposed for the LCL grid-tied inverter where a compound filter in the FUDE consisted of a time delay filter, a zero-phase FIR low-pass filter, and a high-pass filter. With the help of the compound filter, the FUDE acts as a notch filter at the harmonic frequencies when the notch coefficient is reasonably designed. Compared with the conventional UDE with time delay and zero-phase FIR low-pass filter, the proposed FUDE can offer wider notch bandwidths at selected frequencies, which shows the superiority of the proposed FUDE in grid frequency fluctuation adaptability. In addition, according to the small-gain theorem, stability conditions are provided, and the robustness of the proposed controller to the grid impedance variations is analyzed in this article. The effectiveness of the proposed controller has been verified on a 2-kW single-phase grid-tied inverter.

Appendix

A1 Expressions of $g_{low}(z)$ and $g_{hi}(z)$

The zero-phase low-pass filter $g_{\text{low}}(z)$ is a 20th-order FIR filter whose bandwidth is 1570 rad/s, and its coefficients are obtained by executing the MATLAB function "fir1". The coefficients are expressed in Table II.

$g_{\text{hi}}(z)$ is a first-order IIR filter, its expression is given as

$$g_{\text{hi}}(z) = \frac{s}{s+\alpha} \tag{A1}$$

where $\alpha = 1256$ rad/s is selected here.

TABLE II
COEFFICIENTS OF $G_{\mathrm{LOW}}(z)$

k	0	1	2	3	4	5
$h(k)$	0.09832	0.09571	0.08822	0.07676	0.06274	0.0478
k	6	7	8	9	10	
$h(k)$	0.03358	0.02148	0.01249	0.007042	0.005008	

REFERENCES

[1] T. Liu, J. Liu, Z. Liu, and Z. Liu, "A study of virtual resistor-based active damping alternatives for LCL resonance in grid-connected voltage source inverters," *IEEE Trans. Power Electron.*, vol. 35, no. 1, pp. 247–262, Jan. 2020.

[2] W. Wu, Y. Liu, Y. He, H. S.-H. Chung, M. Liserre, and F. Blaabjerg, "Damping methods for resonances caused by LCL-filter-based current-controlled grid-tied power inverters: An overview," *IEEE Trans. Ind. Electron.*, vol. 64, no. 9, pp. 7402–7413, Sep. 2017.

[3] Y. Wu, Y. Ye, Q. Zhao, Y. Cao, and Y. Xiong, "Discrete-time modified UDE-based current control for LCL-type grid-tied inverters," *IEEE Trans. Ind. Electron.*, vol. 67, no. 3, pp. 2143–2154, Mar. 2020.

[4] M. Elkayam, S. Kolesnik, and A. Kuperman, "Guidelines to classical frequency-domain disturbance observer redesign for enhanced rejection of periodic uncertainties and disturbances," *IEEE Trans. Power Electron.*, vol. 34, no. 4, pp. 3986–3995, Apr. 2019.

[5] C. Bao, X. Ruan, X. Wang, W. Li, D. Pan, and K. Weng, "Step-by-step controller design for LCL-type grid-connected inverter with capacitor–current-feedback active-damping," *IEEE Trans. Power Electron.*, vol. 29, no. 3, pp. 1239–1253, Mar. 2014.

[6] H. Gholizade-Narm, S. A. Khajehoddin, and M. Karimi-Ghartemani, "Reduced-order controllers using integrated controller-plant dynamics approach for grid-connected inverters," *IEEE Trans. Ind. Electron.*, vol. 68, no. 8, pp. 7444–7453, Aug. 2021.

[7] Q. Zhao and Y. Ye, "Fractional phase lead compensation RC for an inverter: Analysis, design, and verification," *IEEE Trans. Ind. Electron.*, vol. 64, no. 4, pp. 3127–3136, Apr. 2017.

[8] R. P. Vieira, L. T. Martins, J. R. Massing, and M. Stefanello, "Sliding mode controller in a multiloop framework for a grid-connected VSI with LCL filter," *IEEE Trans. Ind. Electron.*, vol. 65, no. 6, pp. 4714–4723, Jun. 2018.

[9] T. V. Tran, K.-H. Kim, and J.-S. Lai, "Optimized active disturbance rejection control with resonant extended state observer for grid voltage sensorless LCL-filtered inverter," *IEEE Trans. Power Electron.*, vol. 36, no. 11, pp. 13317–13331, Nov. 2021.

[10] N. Alshek, S. Bronshtein, M. Elkayam, and A. Kuperman, "Modified uncertainty and disturbance estimator for enhanced periodic signals suppression," *IEEE Trans. Ind. Electron.*, vol. 66, no. 2, pp. 1246–1254, Feb. 2019.

[11] W.-H. Chen, J. Yang, L. Guo, and S. Li, "Disturbance-observer-based control and related methods– An overview," *IEEE Trans. Ind. Electron.*, vol. 63, no. 2, pp. 1083–1095, Feb. 2016.

[12] B. Ren, Q.-C. Zhong, and J. Dai, "Asymptotic reference tracking and disturbance rejection of UDE-based robust control," *IEEE Trans. Ind. Electron.*, vol. 64, no. 4, pp. 3166–3176, Apr. 2017.

[13] J. Ren, Y. Ye, G. Xu, Q. Zhao, and M. Zhu, "Uncertainty-and-disturbance-estimator-based current control scheme for PMSM drives with a simple parameter tuning algorithm," *IEEE Trans. Power Electron.*, vol. 32, no. 7, pp. 5712–5722, Jul. 2017.

[14] Y. Ye and Y. Xiong, "UDE-based current control strategy for $LCCL$-type grid-tied inverters," *IEEE Trans. Ind. Electron.*, vol. 65, no. 5, pp. 4061–4069, May 2018.

[15] J. Chen, B. Ren, and Q.-C. Zhong, "UDE-based trajectory tracking control of piezoelectric stages," *IEEE Trans. Ind. Electron.*, vol. 63, no. 10, pp. 6450–6459, Oct. 2016.

[16] Q. Zhong and D. Rees, "Control of uncertain LTI systems based on an uncertainty and disturbance estimator," *J. Dyn. Sys. Meas. Control*, vol. 126, no. 4, pp. 905–910, Dec. 2004.

[17] Y. Xiong, Y. Ye, Y. Cao, and Y. Wu, "Separate-structure UDE-based current resonant control strategy on LCL-type grid-tied inverters with weighted average current method for improved injected current quality and robustness," *IEEE Trans. Power Electron.*, vol. 35, no. 12, pp. 13641–13651, Dec. 2020.

[18] S. Y. Gadelovits, Q.-C. Zhong, V. Kadirkamanathan, and A. Kuperman, "Uncertainty and disturbance estimator-based controller equipped with a time-delayed filter to improve the voltage quality of inverters," *IEEE Trans. Ind. Electron.*, vol. 66, no. 1, pp. 459–469, Jan. 2019.

[19] Y. Vule, M. Elkayam, and A. Kuperman, "Uncertainty and disturbance estimator with improved steady-state performance for grid-connected power converters," *IET Renewable Power Gener.*, vol. 14, no. 12, pp. 2183–2191, 2020.

[20] Z.-X. Zou, K. Zhou, Z. Wang, and M. Cheng, "Frequency-adaptive fractional-order repetitive control of shunt active power filters," *IEEE Trans. Ind. Electron.*, vol. 62, no. 3, pp. 1659–1668, Mar. 2015.

[21] J. Wang, J. D. Yan, L. Jiang, and J. Zou, "Delay-dependent stability of single-loop controlled grid-connected inverters with LCL filters," *IEEE Trans. Power Electron.*, vol. 31, no. 1, pp. 743–757, Jan. 2016.

[22] D. Pan, X. Ruan, C. Bao, W. Li, and X. Wang, "Capacitor-current-feedback active damping with reduced computation delay for improving robustness of LCL-type grid-connected inverter," *IEEE Trans. Power Electron.*, vol. 29, no. 7, pp. 3414–3427, Jul. 2014.

[23] M. Liserre, R. Teodorescu, and F. Blaabjerg, "Stability of photovoltaic and wind turbine grid-connected inverters for a large set of grid impedance values," *IEEE Trans. Power Electron.*, vol. 21, no. 1, pp. 263–272, Jan. 2006.

[24] R. W. Longman, "Iterative learning control and repetitive control for engineering practice," *Int. J. Control*, vol. 73, no. 10, pp. 930–954, 2000.

[25] J. Sun, "Impedance-based stability criterion for grid-connected inverters," *IEEE Trans. Power Electron.*, vol. 26, no. 11, pp. 3075–3078, Nov. 2011.

[26] *Requirements for Micro-Generating Plants to be Connected in Parallel With Public Low-Voltage Distribution Networks*, CENELEC. EN 50438, 2013.

Yongkang Xiong was born in Jiujiang, China. He received the B.E. and M.E. degrees in automation and circuits and systems from the East China University of Technology, Nanchang, China, in 2012 and 2015 respectively, and the Ph.D. degree in control theory and control engineering from the Nanjing University of Aeronautics and Astronautics, Nanjing, China, in 2019.

He is currently a Faculty Member with the School of Information Engineering, Nanchang University, Nanchang, China. His research interests include power electronics control and disturbance rejection control technique.

Yongqiang Ye (Senior Member, IEEE) was born in Tongxiang, China. He received the B.E. and M.E. degrees from Zhejiang University, Hangzhou, China, in 1994 and 1997, respectively, and the Ph.D. degree from Nanyang Technological University, Singapore, in 2004, all in electrical engineering.

For more than four years, he was a Faculty Member with the School of Information, Zhejiang University of Finance and Economics, Hangzhou, China. He was also a Postdoctoral Research Fellow with the Department of Electrical Engineering, Lakehead University, Thunder Bay, ON, Canada, the Department of Systems and Computer Engineering, Carleton University, Ottawa, ON, Canada, and the Department of Mechanical Engineering, Dalhousie University, Halifax, NS, Canada. Since 2009, he has been a Professor with the College of Automation Engineering, Nanjing University of Aeronautics and Astronautics, Nanjing, China. He is currently a Distinguished Professor of Henan province affiliated with the School of Electronic and Information, Zhongyuan University of Technology, Zhengzhou, China. He has authored or coauthored one book and more than 75 journal papers. His research interests include advanced control of power electronics and electrical machines.

Mingzhe Zhu was born in Zibo, China. He received the B.E. degree in automation, the M.E. degree in control engineering, and the Ph.D. degree in control theory and control engineering from the Nanjing University of Aeronautics and Astronautics, Nanjing, China, in 2013, 2016, and 2021 respectively.

He is currently a Faculty Member with the School of Electric power Engineering, Nanjing Institute of Technology, Nanjing, China. His research interests include power electronics and advanced control.